A 0.55-Ma paleotemperature record from the Subantarctic zone: Implications for Antarctic Circumpolar Current development

Sabine Becquey[1] and Rainer Gersonde

Alfred-Wegener Institute for Polar and Marine Research, Columbusstrasse, Bremerhaven, Germany

Received 17 August 2000; revised 17 July 2002; accepted 16 September 2002; published 19 March 2003.

[1] Estimates of summer sea surface temperatures (SSSTs) derived from planktic foraminiferal associations using the Modern Analog Technique and combined with isotopic analyses and determination of ice-rafted debris, mirror the Pleistocene evolution of the planktic Subantarctic surface waters in the Atlantic Ocean. The SSSTs indicate that the isotherms that define the modern polar front zone and Subantarctic front, were located at more northerly latitudes (up to 7°) during most of the investigated period, which covers the past 550 kyr. Exceptions are during climatic optima in the early Holocene, at marine isotope stages (MIS) 5.5, 7.1, 7.5, 9.3, and presumably during MIS 11.3 when SSSTs exceeded modern values by 1°–5°C. The close similarity between the SSST and the Vostok temperature indicates strong regional temperature correlation. Both records show that MIS 9.3 was the warmest period during the last 420 kyr whereas SSSTs obtained for MIS 11.3 are overestimated due to strong carbonate dissolution. Spectral analysis corroborates that the initiation of warming in southern high latitudes heralds the start of deglaciation on the Northern Hemisphere. *INDEX TERMS:* 4267 Oceanography: General: Paleoceanography; 4271 Oceanography: General: Physical and chemical properties of seawater; 4299 Oceanography: General: General or miscellaneous; *KEYWORDS:* Subantarctic zone, sea surface temperatures, planktic foraminifers, ice rafted debris, climate

Citation: Becquey, S., and R. Gersonde, A 0.55-Ma paleotemperature record from the Subantarctic zone: Implications for Antarctic Circumpolar Current development, *Paleoceanography*, *18*(1), 1014, doi:10.1029/2000PA000576, 2003.

1. Introduction

[2] The Antarctic Circumpolar Current (ACC) represents the most important junction in the global ocean circulation system. It controls the exchange of nutrients, salt, and heat in the world ocean by linking the Atlantic, the Indian, and the Pacific Oceans, and thus plays an important role in the development of Earth's climate [*Broecker*, 1982a, 1982b; *Keir*, 1988; *Peterson and Stramma*, 1991]. The ACC can be divided into three zones, the Subantarctic zone (SAZ), the polar front zone (PFZ), and the Antarctic zone (AZ), separated by oceanographic frontal systems, the polar front (PF), the Subantarctic front (SAF), and the subtropical front (STF) (Figure 1). Each zone is characterized by specific temperature, salinity, and nutrient regimes [*Lutjeharms and Valentine*, 1984]. The fronts and their associated sea surface temperature (SST) signatures are well reflected by planktic foraminiferal faunas in surface sediments [*Howard and Prell*, 1984; *Labracherie et al.*, 1989; *Thiede et al.*, 1997; *Weaver et al.*, 1997; *Niebler and Gersonde*, 1998] as well as by radiolarian and diatom assemblages [*Pichon et al.*, 1992; *Zielinski and Gersonde*, 1997; *Abelmann et al.*, 1999]. Variations in microfossil assemblage composition reflect changes in the paleolatitudes of the sea surface isotherms of the ACC zones that are related to the Pleistocene climate history, and thus allow deciphering the past Southern Ocean thermal evolution [*Howard and Prell*, 1984, 1992; *Labracherie et al.*, 1989; *Morley*, 1989; *Labeyrie et al.*, 1996; *Brathauer and Abelmann*, 1999; *Waelbroeck et al.*, 1999]. Such knowledge is crucial to our improved understanding of paleoceanographic processes controlling the world ocean circulation pattern.

[3] Here we present micropaleontological, sedimentological, and geochemical data from sediment core PS2489-2 recovered in the central region of the modern SAZ, which document the paleohydrographic variations in the SAZ and the related SAF and STF during the past 550 kyr (marine isotope stage, MIS 1–14). Our study combines the analysis of changes in planktic foraminiferal assemblage composition and foraminiferal fragmentation, variations in the isotopic composition of benthic and planktic foraminifers, and changes in the proportion of ice-rafted debris (IRD). These data were used to reconstruct past summer sea surface temperatures (SSSTs) and to decipher changes in circulation, at a time resolution of 2–2.5 kyr. Our data allow us to study the response of the Southern Ocean to orbital forcing of climate and its phase relationships with climatic change in other regions. The presented data obtained from PS2489-2 can be requested via Internet (www.pangaea.de).

2. Material and Methods

2.1. Core Material and Sample Preparation

[4] Piston core PS2489-2 was recovered during the ANT-XI/2 cruise of "*R/V Polarstern*" [*Gersonde*, 1995] from the

[1]Now at Department of Geology, Faculty of Sciences, University of Salamanca, Salamanca, Spain.

0883-8305/03/2000PA000576

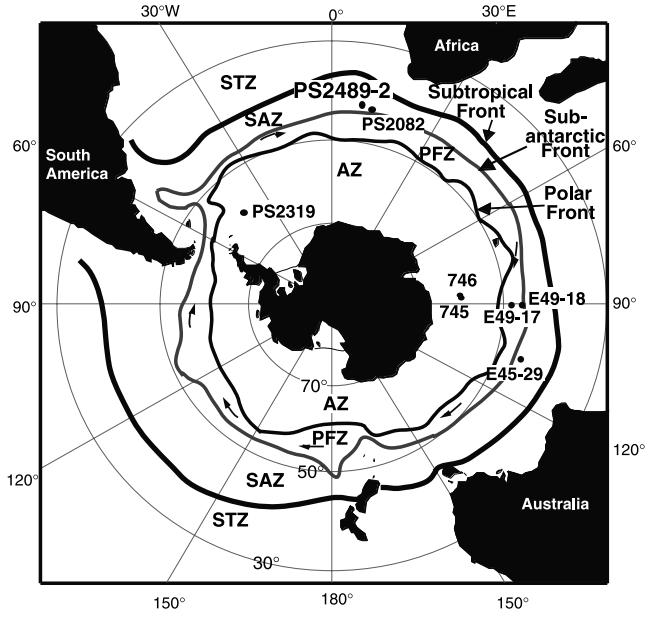

Figure 1. Core locations and positions of the oceanographic fronts. PF, polar front; SAF, Subantarctic front; STF, subtropical front and of the oceanographic zones; AAZ, Antarctic zone; PFZ, polar front zone; SAZ, Subantarctic zone [according to *Peterson and Stramma*, 1991]. Location of winter sea ice edge according to *Sea Ice Climatic Atlas* [1985].

southern Agulhas Fracture Zone Ridge (42°52.4′S, 8°58.4′E). This site is located in the central region of the SAZ (Figure 1), where present SSSTs are about 10°C at 10 m of water [*Levitus and Boyer*, 1994]. The water depth at the core location (3794 m) is near the boundary between the North Atlantic deep water and the underlying circumpolar deep water [*Olbers et al.*, 1992], and above the carbonate compensation depth.

[5] The core is 12.84 m long and the sediments consist of alternating foraminiferal mud and ooze [*Gersonde*, 1995]. The sediments close to the sediment surface are documented in a 0.78-m long trigger core (PS2489-2TC) that overlaps in its lower portion with the top section of the piston core. Samples for microfaunal analysis were taken every 5 cm in most parts of the core. Sampling interval of 3–4 cm was used for MIS 2–4 due to a lower sedimentation rate during this time interval.

2.2. Micropaleontological Analysis

[6] Samples were washed through a 63-μm sieve. Planktic foraminifers were identified and counted in the dried sample residue >125 μm following the method of *Pflaumann et al.* [1996] (see *Becquey and Gersonde* [2002]). Descriptive statistics for planktic foraminifers from core PS2489-2 are illustrated in Table 1.

[7] To quantify the varying degree of carbonate dissolution affecting the composition of the foraminiferal assemblages we applied the foraminiferal fragmentation ratio proposed by *Le and Shackleton* [1992]: fragments % = 100% × (number fragments/8)/((number fragments/8) + number whole). By assuming that one whole foraminifer can break into several fragments we used this formula rather than the conventional fragmentation index where one fragment is regarded as equal in value to one whole foraminifer. Fragmentation was estimated by counting the number of fragments in a split that contained 500 or more whole planktic foraminifers in the >125 μm fraction.

[8] Lithic fragments in the >125 μm fraction were also counted in order to document fluctuations in the delivery of IRD. Data on recent iceberg observations (1983–2000)

Table 1. Descriptive Statistics for Planktic Foraminifera From Core PS2489-2 With the Average, the Standard Deviation, the Minimum, and Maximum of Each Species

Species	Average	Standard Deviation	Minimum	Maximum
Globigerina bulloides	16.20	9.82	0.78	49.78
Globigerina falconensis	1.23	1.10	0.00	4.36
Globigerinella aequilateralis	0.01	0.05	0.00	0.5
Globigerinella calida	0.09	0.18	0.00	1.01
Globigerinella digitata	0.01	0.05	0.00	0.59
Globigerinita bradyi	1.65	2.27	0.00	15.73
Globigerinita glutinata	5.88	3.53	0.02	18.96
Globigerinoides ruber	0.00	0.03	0.00	0.38
Globorotalia truncatulinoides (D)	0.01	0.04	0.00	0.48
Globorotalia truncatulinoides (S)	0.54	1.01	0.00	6.73
Globorotalia crassaformis	1.33	2.08	0.00	14.69
Globorotalia hirsuta	0.03	0.12	0.00	1.35
Globorotalia inflata	5.98	6.62	0.01	36.78
Globorotalia scitula	0.34	0.58	0.00	3.54
Globoturborotalita rubescens	0.01	0.11	0.00	1.38
Globoturborotalita tenella	0.00	0.02	0.00	0.34
Neogloboquadrina p-d intergrade	0.03	0.16	0.00	1.60
Neogloboquadrina pachyderma (D)	7.32	5.56	0.06	30.60
Neogloboquadrina pachyderma (S)	51.51	19.37	11.63	92.58
Orbulina universa	0.06	0.19	0.00	1.46
Tenuitella iota	0.20	0.50	0.00	2.67
Turborotalita quinqueloba	7.59	4.82	0.00	22.86
Globorotalia theyeri	0.00	0.03	0.00	0.45

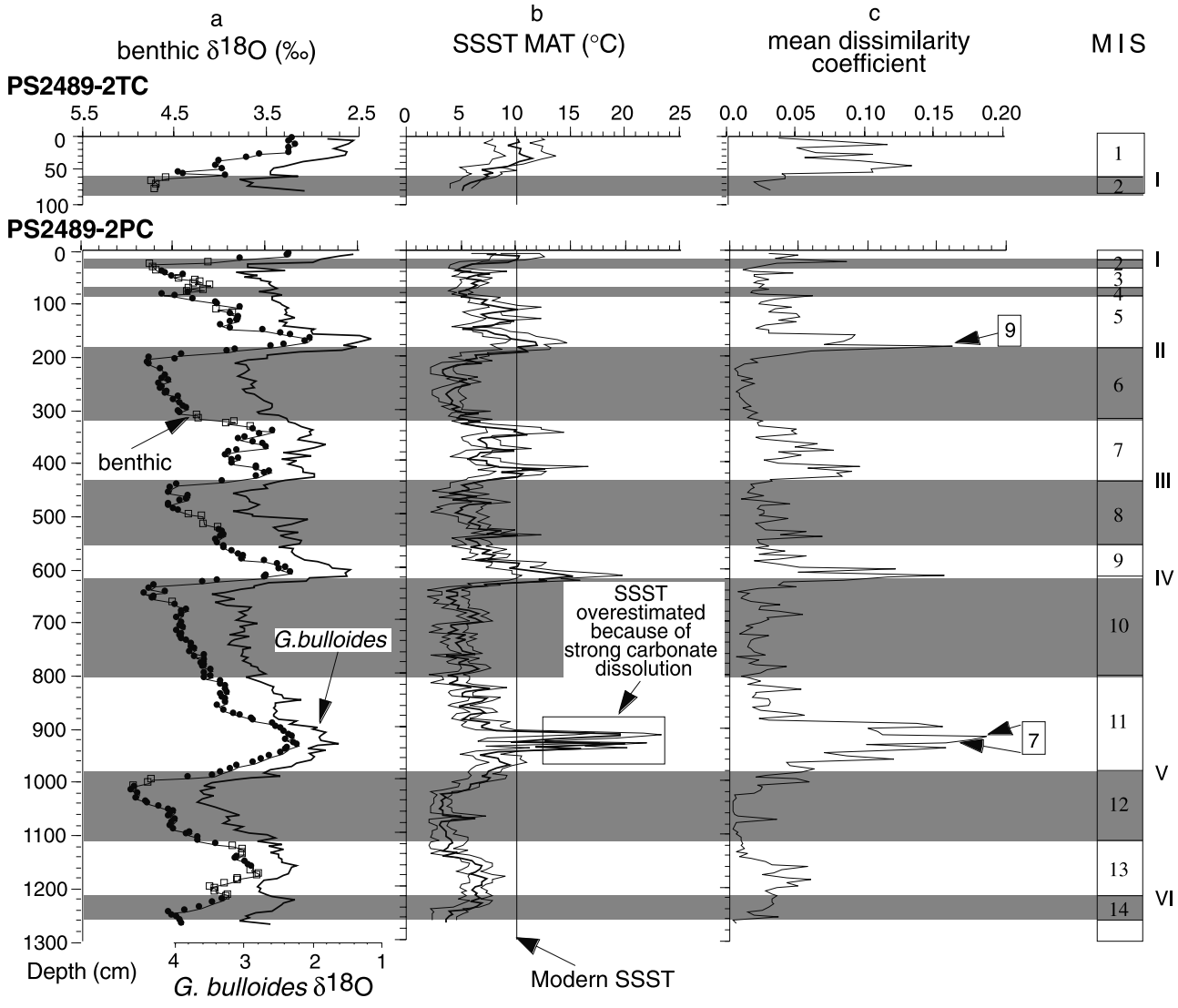

Figure 2. (a) Variations with depth in the trigger core (PS2489-2TC) and piston core (PS2489-2PC) of benthic and planktic foraminiferal $\delta^{18}O$. The benthic $\delta^{18}O$ record is based on analysis of *Cibicidoides* (solid circles) and *U. peregrina* (squares). Data are reported with the correction for specific fractionation: +0.64‰ for *Cibicidoides* [*Shackleton*, 1974]. (b) SSST estimates calculated using the MAT (dark line) and the standard deviation (gray lines). The vertical line indicates the modern SSST of 10.2°C at the core location, according to *Levitus and Boyer* [1994]. (c) The mean dissimilarity coefficient for 10 best modern analogs (note that for three samples, during MIS 5.5 and MIS 11.3 only nine and seven analogs were found to estimate the SSST). Shaded areas mark glacial periods. Terminations I–VI are labeled.

have been retrieved from the *Polarstern* database available at http://www.awi-bremerhaven.de/MET/Polarstern/poldat.html.

2.3. Estimation of SSST

[9] To calculate the temperature estimates, we chose the Modern Analog Technique (MAT), using a program adapted by *Sieger* [1995] and *Sieger et al.* [1999] for Macintosh computers. The MAT [*Hutson*, 1980; *Prentice*, 1980; *Overpeck et al.*, 1985] matches a down-core sample with surface sediment samples, which have a similar microfossil composition using a dissimilarity coefficient. The estimates are based on an average of measurements for the subset of modern samples, weighted by their similarity index [*Hutson*, 1980]. In this method, the sample which has a smaller dissimilarity coefficient (or higher similarity index) contributes more to the SST estimate. We selected a maximum of 10 analogs and only considered analogs with a dissimilarity coefficient between 0 (identical, represents a 100% similarity between the modern microfossil composition of a surface sediment sample and a down-core sample microfossil assemblage) and 0.2 (80% similarity) for the SSST estimations (Figure 2), because they give the best results on the modern model (lowest residual temperatures and stand-

Table 2. Results of the Accelerator Mass Spectrometry ^{14}C Dating of Planktic Foraminifers[a]

Core/Depth, cm	Planktic Species	HB N.	Kiel N.	Age, kyr	Age Error	Corrected Ages
			PS2489-2-TC			
1.5	*G.bulloides*	HB 322	KIA 4057	2.3	±50	1.86
21.5	*G.bulloides*	HB 628	KIA 7248	7.42	±50	6.98
41.5	*G.bulloides*	HB 319	KIA 4055	12.2	±90	11.76
76.5	*N.pachyderma sin*	HB 626	KIA 7226	15.6	±80	15.16
			PS2489-2-PC			
4	*G.bulloides*	HB 329	KIA 4064	4.33	±50	3.89
9	*G.bulloides*	HB 349	KIA 4086	7.28	±40	6.84
14	*G.bulloides*	HB 348	KIA 4085	9.12	±50	8.68
19	*G.bulloides*	HB 347	KIA 4084	11.6	±60	11.16
24	*G.bulloides*	HB 343	KIA 4074	15.14	±130	14.7
34	*G.bulloides*	HB 341	KIA 4072	18.17	±170	17.73
38	*G.bulloides*	HB 340	KIA 4071	30.08	+660/−610	29.64
44	*N.pachyderma sin*	HB 627	KIA 7227	33.97	+620/−570	33.53
48	*G.bulloides*	HB 336	KIA 4068	37.7	+1870/−1510	37.26
54	*G.bulloides*	HB 335	KIA 4067	40.8	+2840/−2090	40.36

[a]The ^{14}C-AMS datings have been corrected for 440 years [*Bard*, 1988].

ard deviation). The standard deviation of the temperatures associated with the analogs indicates the range of temperatures associated with a particular modern microfossil assemblage (Figure 2). Imprecise SSST estimates are revealed by the choice of modern analogs with a wide range of temperature values resulting in a high standard deviation.

[10] The reference database consists of 186 surface sediment samples from the South Atlantic and South Indian Oceans, between 20°S and 58°S and includes 26 foraminiferal taxa and taxa groups (H. S. Niebler et al., manuscript in preparation, 2003). The foraminifers considered for SSST estimations are exclusively taxa known to be surface water dwellers [*Niebler et al.*, 1999; *Becquey and Gersonde*, 2002].

[11] The modern SSTs were extracted from *Levitus and Boyer* [1994]. They correspond to the mean SSST (January to March) at 10 m water depth. We chose to reconstruct SSST because the microplankton flux, including foraminifers, is strongly focused on austral summer in southern high-latitude areas, as documented by sediment trap experiments [*Abelmann and Gersonde*, 1991; *Wefer et al.*, 1988; *Wefer and Fischer*, 1991; *Donner and Wefer*, 1994; *Fischer et al.*, 2002].

2.4. Isotope Analysis and Age Model

[12] The stratigraphic framework was established using a combination of Accelerator Mass Spectrometry (AMS)^{14}C dating and oxygen isotope stratigraphy based on benthic foraminifers. In total, 14 AMS^{14}C ages were obtained from the trigger core and the top half meter of the piston core. The ages were measured on monospecific samples of the planktic foraminifers *Globigerina bulloides* and *Neogloboquadrina pachyderma* sin. (size fraction 200–250 μm) (Table 2). The ages have been corrected for a constant surface water age of 440 years, the estimated prebomb age of the surface water at 43°S [*Bard*, 1988]. The samples were measured in the Kiel Leibnitz-Labor AMS facility (3MV HVEE Tanderon 4130 AMS) [*Nadeau et al.*, 1997].

[13] Benthic (*Uvigerina peregrina*, *Fontbotia wuellerstorfi*, and species of the related genus *Cibicidoides*) and planktic (*G. bulloides*) foraminifers were picked for isotope analysis. The isotope measurements were made using a Finnigan MAT 251 mass spectrometer coupled to an automatic carbonate preparation device in the Alfred Wegener Institute. Data are related to the PDB standard through repeated analyses of National Bureau of Standard isotopic reference material 19 [*Hut*, 1987]. The standard deviation of repeated analysis of our laboratory carbonate standard run on different days is 0.03‰ for $\delta^{18}O$.

[14] The benthic foraminiferal $\delta^{18}O$ record has been combined from both *F. wuellerstorfi* (and *Cibicidoides* spp.) and *U. peregrina* $\delta^{18}O$ data after correction for specific fractionation (+0.64‰ for *F. wuellerstorfi* and *Cibicidoides* spp. according to *Shackleton*, [1974]) to produce a continuous record (Figure 2a). Our benthic foraminiferal $\delta^{18}O$ records from the piston core PS2489-2 and its trigger core PS2489-2TC, were graphically correlated with the SPECMAP stacked record [*Imbrie et al.*, 1984] using the Analyseries software [*Paillard et al.*, 1996] (Figure 3). The correlation coefficient between both records of benthic foraminiferal $\delta^{18}O$ of PS2489-2 and SPECMAP $\delta^{18}O$ is 0.97 for the trigger core and 0.93 for the piston core. The benthic foraminiferal $\delta^{18}O$ of the composite core was obtained from the combination of the benthic foraminiferal $\delta^{18}O$ of piston core and of the trigger core. The final age scale (Figure 3) was estimated by linear interpolation between the tie points (Table 3) obtained from the graphical correlation.

[15] The sedimentation rate is relatively constant along the core at 2.0–2.5 cm/kyr, with the exception of the top of MIS 2 and during MIS 10 where rates increase to around 11 and 8 cm/kyr, respectively. Our sample spacing of ca. 5 cm, produces a time resolution of 2000–2500 years between each sample, which improves to <1000 years during MIS 10. According to the AMS^{14}C ages one hiatus occurs in the top of the core, which spans between ca. 30 and 18 kyr (late MIS 3 to early MIS 2).

2.5. Spectral Analysis

[16] To determine interhemispheric relation (time lag and leads between the Northern and Southern Hemispheres),

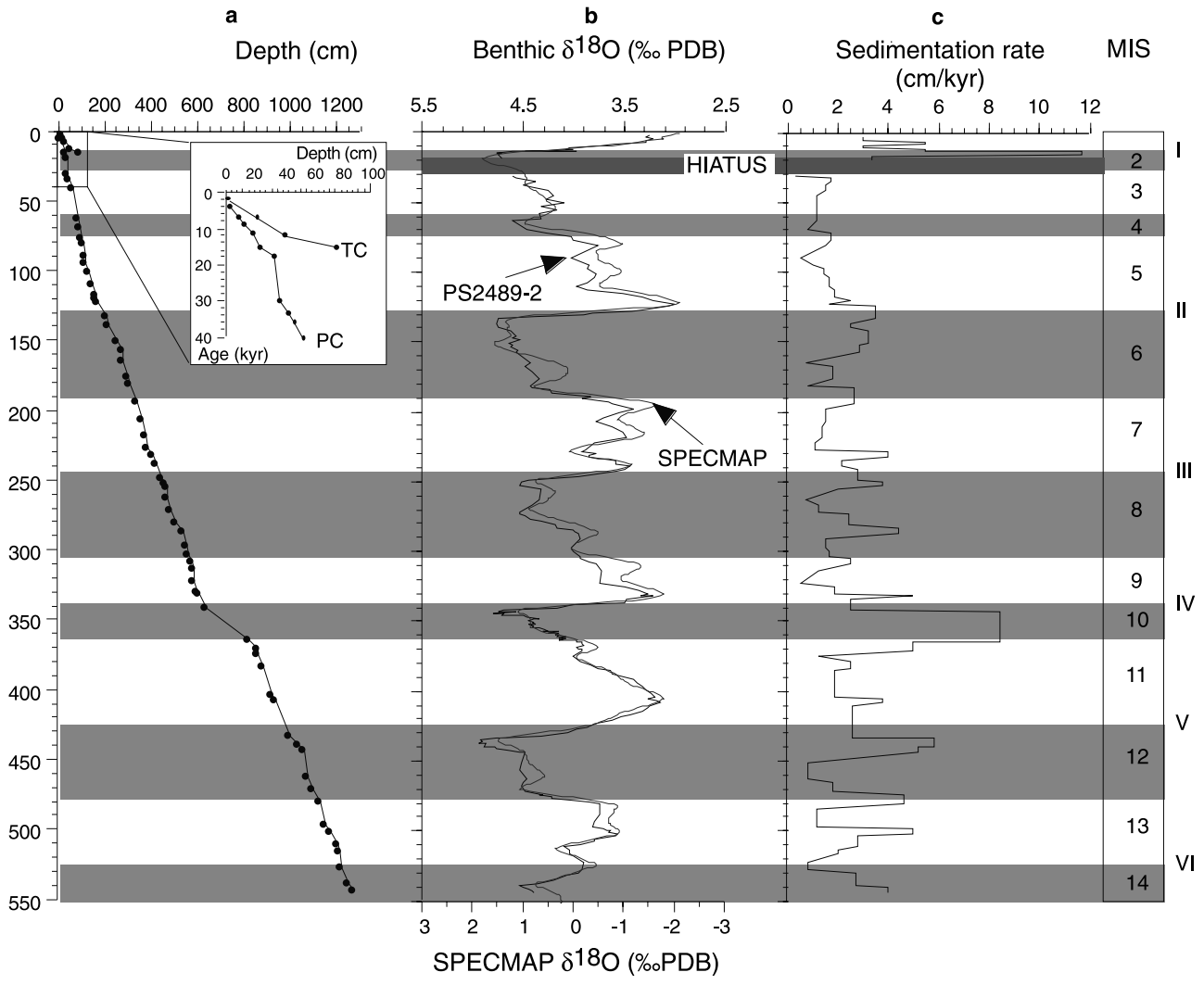

Figure 3. Age model. (a) Age-depth relationship, with the pointers derived from graphic correlation between the benthic foraminiferal $\delta^{18}O$ from the core PS2489-2 and SPECMAP [*Imbrie et al.*, 1984]. The inset for the last 40 kyr shows the ^{14}C-AMS dating used (solid circles) for the trigger core (TC) and the piston core (PC). (b) Benthic $\delta^{18}O$ of the composite core PS2489-2 (dark line) and SPECMAP (gray line) [*Imbrie et al.*, 1984] versus age after the final correlation (see text). (c) Variations in sedimentation rate, shaded areas mark glacial periods. Terminations I–VI are labeled.

cross-spectral analyses were performed on the different proxies of the core PS2489-2. The cross-spectral analysis was done using the Blackman-Tukey method [*Jenkins and Watts*, 1968], using the software Analyseries [*Paillard et al.*, 1996]. Because of the hiatus occurring in the upper part of the sediment core, the spectral analysis was done between 30 and 542 kyr. All time series have been transformed to equidistant sample intervals (2.0 kyr) via linear interpolation. The analysis was performed on the frequency range 0–0.1 kyr^{-1} with a Barlett-type window (30% lags and a 0.0097 kyr^{-1} bandwidth for the planktic $\delta^{18}O$, SSST, and IRD and 50% lags and a 0.0058-kyr^{-1} bandwidth for the foraminiferal fragmentation ratio). Coherency and phases of reversed planktic $\delta^{18}O$, SSST, reversed IRD, and reversed foraminiferal fragmentation ratio have been calculated against the reversed benthic $\delta^{18}O$ used as an indicator for global ice volume. Therefore minima of global ice volume (high $\delta^{18}O$ after reversal) are related with warm SSSTs, low IRD input, and low carbonate dissolution.

3. Results

3.1. SSST Estimates

[17] Two distinct modes of temperature variability are observed in the SSST record obtained for the past 550 kyr (Figure 4a). Between MIS 14 and MIS 12 (550–423 kyr) SSST values show the lowest glacial temperatures (ca. 3°C) and low glacial/interglacial variability around 4°C. The following period is characterized by stronger glacial/interglacial variability. Strongest temperature variations, of up to 16°C, occur during the MIS 12/11 and MIS 10/9 transitions. During MIS 11 and MIS 9 the estimated SSSTs are as high

Table 3. Pointers for Correlation of the Trigger Core PS2489-TC2 and Piston Core PS2489-2PC With the SPECMAP Record [*Imbrie et al.*, 1984]

PS2489-2-TC		PS2489-2-PC	
Depth, cm	Time, ka	Depth, cm	Time, ka
1.5	2	4	4
10.5	5	9	7
21.5	7	14	9
41.5	12	19	11
76.5	15	24	15
		34	18
		38	30
		44	33.5
		48	37
		54	40
		80	62
		85	68
		99	76
		105	80
		109	88
		114	93
		124	100
		139	109
		154	117
		159	119
		164	122
		199	132
		214	138
		249	149
		269	156
		274	163
		296	175
		300	180
		334	193
		354	206
		379	226
		399	231
		414	238
		439	247
		454	251
		460	254
		465	261
		476	270
		498	279
		529	286
		544	296
		554	302
		569	308
		574	312
		579	321
		594	329
		604	331
		629	341
		814	363
		849	370
		854	374
		874	382
		914	403
		929	407
		994	432
		1029	438
		1055	443
		1069	461
		1087	471
		1124	479
		1144	496
		1169	501
		1194	510
		1204	515
		1214	527
		1244	538
		1264	543

as 19° and 15°C, respectively, and thus reach values up to 9°C above the modern SSST at the core location. During the glacial stages MIS 10 and MIS 8, the SSSTs drop to values around 5°C, about 5°C below the modern SSST. The glacial/interglacial cycles above MIS 9 are characterized by less SSST contrast, ranging between 7° and 9°C. Only during the warm interstadials of MIS 7 and MIS 5 (7.5, 7.1, 5.5) and the early Holocene, are the estimated SSSTs slightly warmer than modern temperatures above the core site (10.2°C). The SSST estimates show that MIS 6 is the coldest period during the last 300 kyr with temperatures that are 6°–7°C colder than at present.

[18] In general, the calculated standard deviation of the analogs used for each SSST estimate ranges between 1° and 2°C (Figure 2b). The lowest standard deviations around 1°C were obtained for glacial periods. Rather high standard deviations occur during the climatic optima, being highest during MIS 11.3 and MIS 9.3. This is consistent with the pattern of the mean dissimilarity coefficient that increases during warm interglacials to around 0.15, which represents a similarity between the picked reference samples and the down–core sample of 85% of the foraminiferal signal. Increases of the dissimilarity coefficient in these periods might be related to the relatively low number of reference samples documenting temperate to warm surface water conditions. Only 30 out of 186 samples included in the used reference set are related to temperatures between 10° and 20°C. During cold periods characterized by high values of *N. pachyderma* sin. (70–90%)(Figure 4c), the dissimilarity is close to 0, representing a 100% similarity between the reference and the down-core samples (Figure 2c). Generally, for all down-core samples 10 reference samples with a dissimilarity coefficient <0.2 could be selected. This shows that the reference data set reflects well the down-core variability of foraminiferal assemblages recorded in PS2489-2 and no true "no-analog" situations occur. Less similarity was found in three samples from MIS 11 and MIS 5, where only seven and nine reference samples could be selected for the SSST estimation. Especially, the estimations obtained for the two MIS 11 samples bear highest standard deviations, both being characterized by highest values (35%) of the robustly calcified warm-water dweller *Globorotalia inflata* (Figure 4e). This pattern points to the question how strong and during which time intervals dissolution may have affected and biased the obtained SSST estimates.

[19] The degree of dissolution affecting the foraminiferal assemblages can be documented by the foraminiferal fragmentation index and by the ratio of species that are more and less resistant to carbonate dissolution (Figure 4). Distributions of two dissolution-resistant species, the cold-water taxon *N. pachyderma* sin. and the typical warm-water taxon, *G. inflata*, and the dissolution-sensitive taxon *G. bulloides* [*Berger*, 1968, 1970; *Thunell and Honjo*, 1981], a species that is related to water temperatures between 10° and 16°C [*Niebler and Gersonde*, 1998 and references therein] have been used.

[20] In general, the fragmentation ratio reveals that low fragmentation/dissolution is confined to the warmest interstades and strongest fragmentation occurs during glacial periods. This pattern, corresponding to the "Atlantic-type"

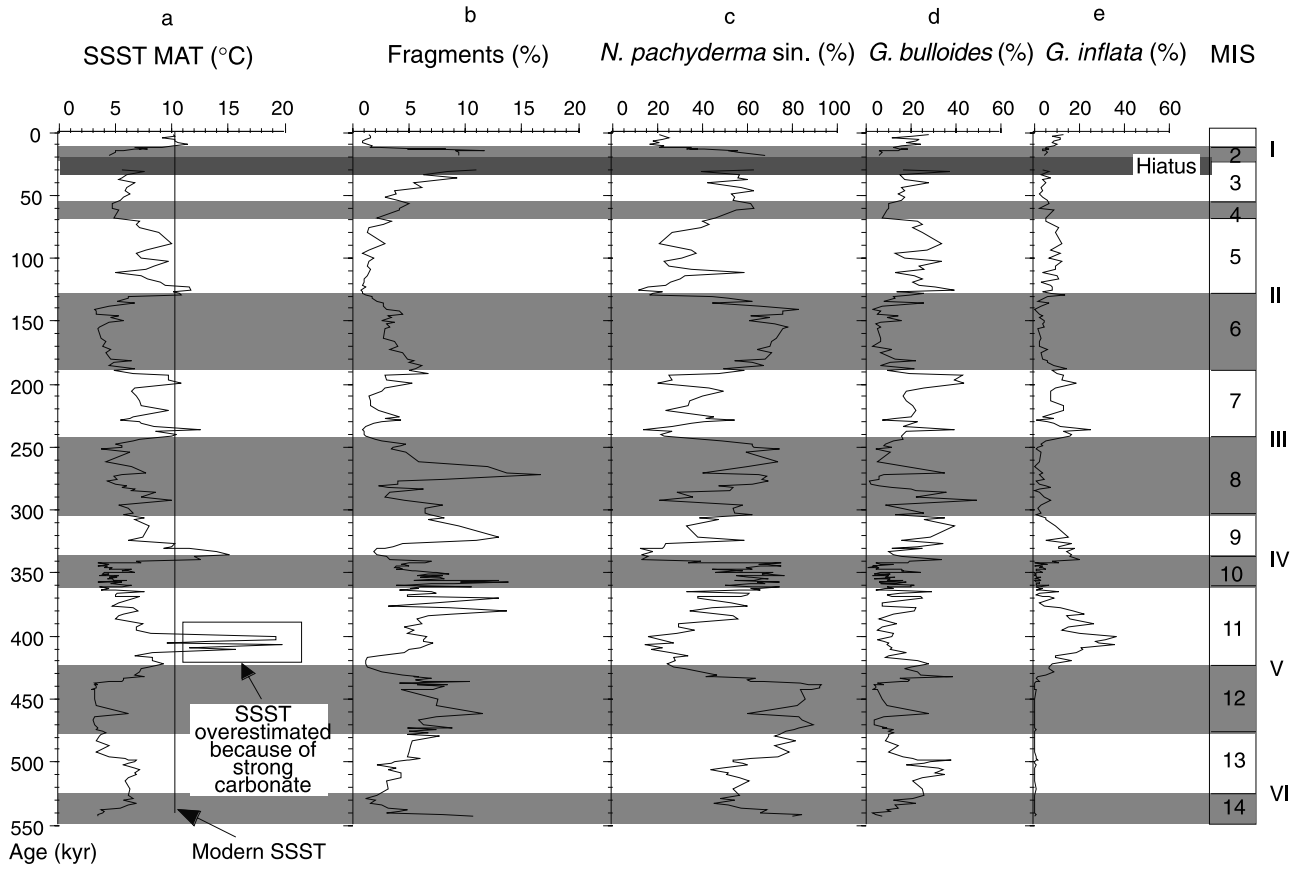

Figure 4. Time series of (a) SSST estimated, (b) percent of planktic foraminiferal fragments, and the relative abundance of the major planktic foraminifers *N. pachyderma* sinistral coiling, (c) *G. bulloides*, and (d) *G. Inflata.* (e) Shaded areas mark glacial periods. Terminations I–VI are labeled.

carbonate pattern, was previously shown in core TTN057-6 [*Hodell et al.*, 2001] located close to core PS2489-2. However, between MIS 13 and MIS 9 this pattern is more intricate. In this interval we observe good carbonate preservation restricted to the terminations and increased dissolution to occur during interglacials. In general, higher fragmentation values are associated with high percentages of *N. pachyderma* sin. and low percentages of *G. bulloides*, a pattern which leads to a strong decrease of SSST during the late MIS 13 and MIS 11 (Figure 4). During MIS 11.3, the increase of the fragmentation ratio associated with increased occurrences of *G. inflata* and a strong decrease of *G. bulloides* (Figure 4) led us to interpret the foraminiferal assemblage as also strongly affected by carbonate dissolution. During most interglacials, the abundant increase of *G. inflata* is due to the establishment of warm-water environments and its occurrence in the sediment record is not biased by dissolution as indicated by the cooccurring increase of *G. bulloides* and a low fragmentation ratio. Only MIS 11.3 shows high percentages of *G. inflata* associated with high fragmentation index. This dissolution related increase of *G. inflata* might have caused overestimated SSST values during MIS 11.3. *Hutson* [1977] documented a similar effect from MIS 11 sections in cores recovered in the Indian Ocean. Also, considering that the Vostok atmospheric temperatures [*Petit et al.*, 1999], as well as other sea surface water records from the Southern Ocean and the North Atlantic [*Oppo et al.*, 1998; *McManus et al.*, 1999; *Waelbroeck et al.*, 1999; *Bauch et al.*, 2000; *Hodell et al.*, 2000; *Kunz-Pirrung et al.*, 2002.] did not result in MIS 11 temperatures that exceed the values obtained from the interglacial periods of the past 350 kyr, we conclude that our MIS 11.3 estimates are unrealistic and must be reduced by up to 6°–7°C.

[21] To check independently if our glacial SSST estimates are lowered by increased numbers of *N. pachyderma* due to selective dissolution we compared the estimated SSST values with the occurrence of IRD, an indicator for the presence of icebergs. This shows that highest IRD values are related to a temperature range up to 4°–5°C. Modern iceberg distribution data compiled from a 18-year survey in the Atlantic sector of the Southern Ocean indicate that the northern limit of iceberg occurrence is associated with a surface water temperature around 4°C (Figure 5), corresponding to the southern PFZ. Because of the rapid temperature increase within the PFZ [*Lutjeharms and Valentine*, 1984], this boundary serves as a barrier to the northward drift of most Southern Ocean icebergs. SSST values derived from radiolarian assemblages in core PS2082-1, recovered in the Agulhas

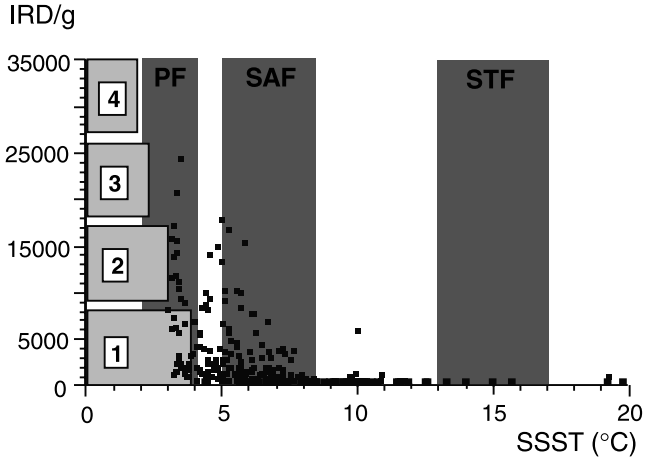

Figure 5. Distribution of the IRD versus the SSST. Oceanographic fronts shaded and labeled are PF, polar front; SAF, Subantarctic front; and STF, subtropical front. The horizontal boxes delimited the present-day distribution of icebergs versus SSST in the South Atlantic (see text) with (1) 1–5 icebergs with or without growlers and bergy bits, (2) 6–10 icebergs with or without growlers and bergy bits, (3) 11–20 icebergs with or without growlers and bergy bits, and (4) more than 20 icebergs with growlers and bergy bits.

Basin ca. 230 km east of PS2489-2 (Figure 1), result in glacial temperatures around 5°C [*Brathauer and Abelmann*, 1999], close to the range of our glacial temperatures obtained with foraminiferal assemblages. Both the comparison with the IRD and the radiolarian estimates indicate that despite increased fragmentation the preserved foraminiferal assemblages reflect well the glacial SSST values.

3.2. Time Series Analyses

[22] The 550 kyr record of core PS2489-2 allows us to generate power spectra and study the phase relationships between Southern Ocean SSSTs and other climate proxies. The confidence levels for phases and coherencies were at 80% for all calculations (with ΔArctanh(Coh) 80% = 0.40 for the planktic $\delta^{18}O$, SSST, and IRD, and ΔArctanh(Coh) 80% = 0.52 for the foraminiferal fragmentation ratio [*Jenkins and Watts*, 1968]). Isotopic, SSST, and IRD records show variance peaks in the 1/100, 1/41, and 1/23 kyr^{-1} frequency ranges of the Milankovitch bands (Figure 6 and Table 4). The power spectra show highest concentration of variance in the 100 kyr band for these variables. SSSTs lead the benthic foraminiferal $\delta^{18}O$ by about to in the eccentricity cycle, in the obliquity cycle, and in the precession cycle. The lead of SSSTs observed in PS2489-2 is of the same order as that found in other Southern Ocean cores [*Howard and Prell*, 1992; *Labeyrie et al.*, 1996; *Brathauer and Abelmann*, 1999; *Waelbroeck et al.*, 1999]. This corroborates that the initiation of warming in southern high latitudes heralds the start of deglaciation in the Northern Hemisphere. In contrast, the planktic $\delta^{18}O$ is more or less in phase with the benthic $\delta^{18}O$. This can be interpreted that in PS2489-2 the planktic $\delta^{18}O$ signal is strongly influenced by ice volume changes and less dependent on fluctuations of the SSST.

4. Discussion

4.1. Southern Ocean Pleistocene Surface Water Temperature Records

[23] The SSST record enables us to reconstruct the location of and the latitudinal shifts in the isotherms related to the ACC in the southern Atlantic during the past 550 kyr. This assumes that the definition of modern oceanic frontal systems can be applied for paleoceanographic reconstructions. However, such an assumption should be treated with caution, because during glacial periods the composition and circulation of water masses in the global ocean that influence Southern Ocean hydrography were different from modern conditions [*Duplessy and Shackleton*, 1985; *Boyle and Keigwin*, 1987; *Labeyrie et al.*, 1987; *Oppo and Fairbanks*, 1987; *Duplessy et al.*, 1988; *Curry et al.*, 1988; *Raymo et al.*, 1990; *Sarnthein et al.*, 1994]. Our reconstruction suggests that during most of the past 550 kyr the SSSTs above the core location were lower than the ones at present (Figure 7a). Only during climatic optima in the early Holocene and at MIS 5.5, 7.1, 7.3, 9.3, and presumably also during MIS 11.3, have the SSSTs exceeded the modern SSST by 1°–5°C (Figures 7a and 8b). This was also observed in cores with lower time resolution from the

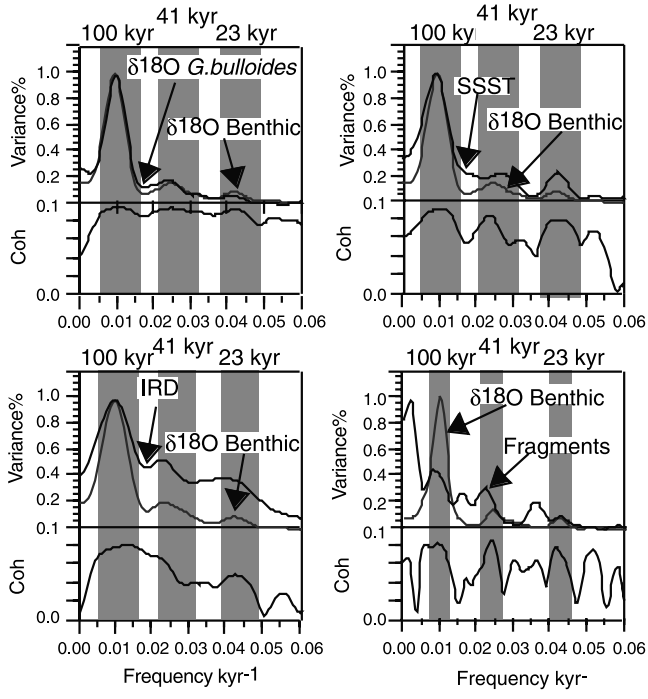

Figure 6. Results of cross-spectral analysis between the reversed benthic foraminiferal $\delta^{18}O$ (gray line) and the reversed planktic foraminiferal $\delta^{18}O$, the SSST record, the reversed foraminiferal fragmentation ratio, and the reversed IRD record of the core PS2489-2. The variance power is expressed as percentage of the total variance. Shaded areas are equal to a bandwidth of 1.

Table 4. Results of Cross-Spectral Analyses[a]

	1/100 kyr^{-1}			1/41 kyr^{-1}			1/23 kyr^{-1}		
Data	*k*	phi	ka	*K*	phi	ka	*k*	Phi	ka
SSST 542	0.93	−22.9 ± 7.8	−6.5 ± 2.3	0.82	−13.2 ± 14.5	−1.5 ± 1.6	0.82	−45.1 ± 14.5	−2.9 ± 0.9
SSST 450	0.95	−17.4 ± 6.7	−4.9 ± 1.9	0.81	−15.2 ± 14.5	−1.6 ± 1.6	0.79	−46.4 ± 15.9	−3.0 ± 1.1
SSST 350	0.95	−11.6 ± 6.9	−3.3 ± 1.9	0.86	−24.4 ± 11.9	−2.7 ± 1.3	0.91	−48.5 ± 9.2	−3.2 ± 0.6
δ^{18}O *G. bulloides*	0.97	−2.9 ± 4.6	−0.8 ± 1.3	0.97	−13.6 ± 4.8	−1.5 ± 0.5	0.95	−0.8 ± 6.7	−0.1 ± 0.4
Fragmentation ratio	0.85	−51.7 ± 35.9	−14.3 ± 9.9	0.89	−60.4 ± 47.1	−6.7 ± 5.2	0.80	38.6 ± 57.5	2.5 ± 3.7
IRD	0.81	−3.2 ± 17.7	−0.8 ± 4.9						

[a]Variables are crossed with the reversal benthic foraminiferal δ^{18}O. Presented are the coherencies (*k*), the phase angles (phi) and the phase time (kyr). Positive (negative) phases indicate that a variable lags (leads) the benthic foraminiferal δ^{18}O. Concerning the SSST record, cross-spectral analyses were performed for the last 542 kyr (SSST 542), for the last 450 kyr (SSST 450), and for the last 350 kyr (SSST 350). Note that in these three cases, the phase shows strong variations for the eccentricity cycle.

Atlantic [*Gersonde et al.*, 1996; *Brathauer and Abelmann*, 1999], Indian [*Howard and Prell*, 1984; *Pichon et al.*, 1992; *Labeyrie et al.*, 1996], and the Pacific [*Weaver et al.*, 1998] sectors of the Southern Ocean.

[24] This pattern can be interpreted to indicate that the ACC zones and related oceanic frontal systems were shifted to a more northward position by up to 7° latitude. During glacial periods the SSST dropped to values comparable to those around the modern polar front (Figure 8c). As a consequence, icebergs that are generally limited to the southern PFZ at present (at about 50°S [*Lutjeharms*, 1985]) (Figure 5) could invade the area presently occupied by the central SAZ. This is indicated by the presence of IRD in sediments of glacial intervals (Figures 7e and 8c). However, IRD cannot be explained solely in terms of temperature. In fact, the amount of IRD is controlled by

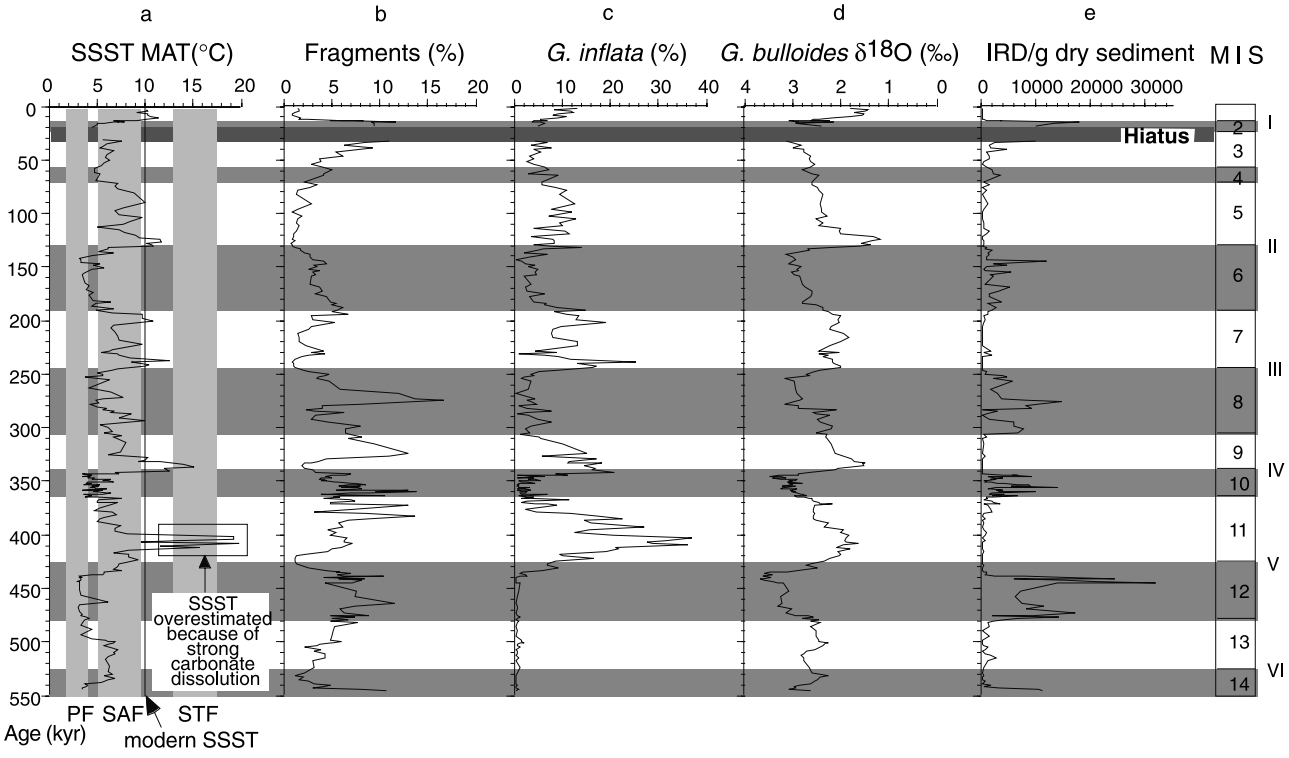

Figure 7. (a) Comparison of the variations of SSST during the last 550 kyr with the present temperature range of the polar front (PF), Subantarctic Front (SAF), and the subtropical front (STF). Note that only during the warmest interglacial periods the SSST were higher than the present-day SSST (vertical line). (b) Distribution of the percent of fragments. The percentage fragments record shows two periods, high dissolution between MIS 14 and MIS 8 and lower dissolution for the upper part. (c) Percent of *G. inflata*. Note the rare presence of *G. inflata* from MIS 14 to MIS 12. (d) The *G. bulloides* δ^{18}O record. (e) Distribution of IRD. The IRD/g record displays a long-term trend of decreasing IRD in progressively younger glacials. Note the hiatus (diagonal lines) separating late MIS 3 and early MIS 2. Shaded areas mark glacial periods. Terminations I–VI are labeled.

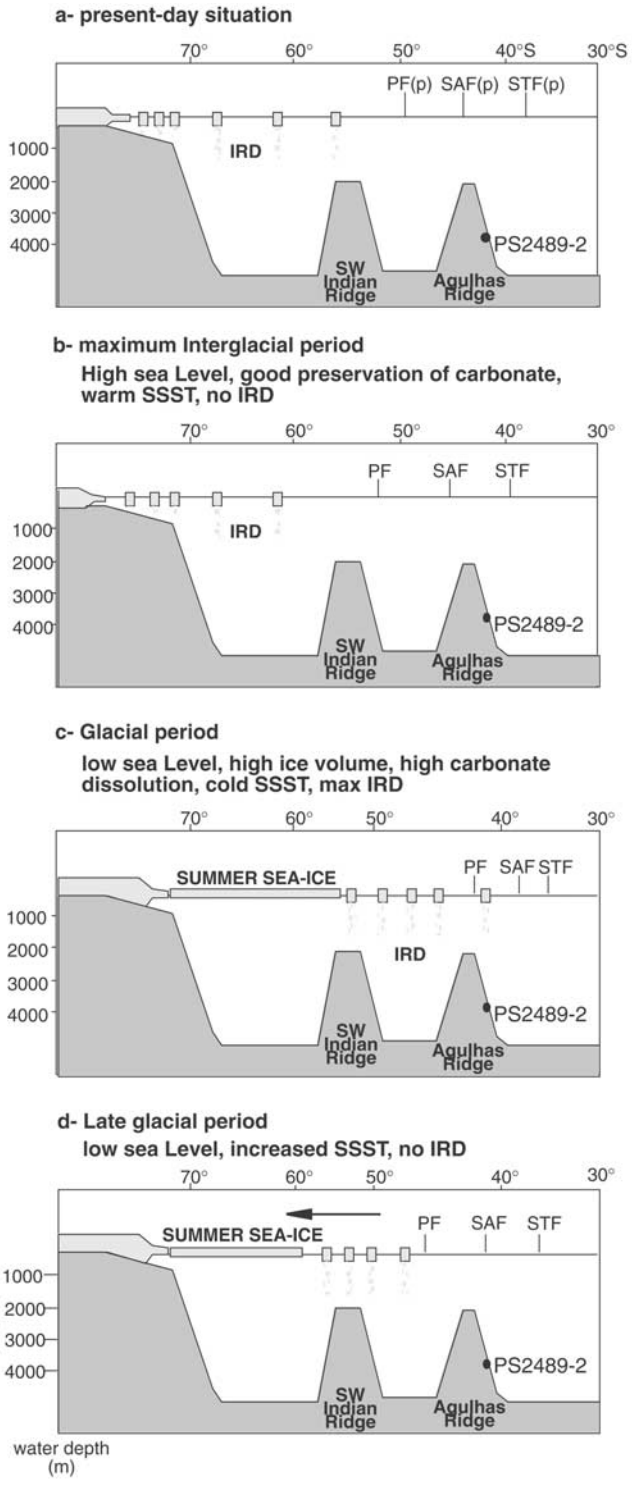

Figure 8. Schematic model of surface environments in the South Atlantic during (a, b) interglacial and (c, d) glacial periods. PF(p), SAF(p), and STF(p) correspond to the present-day position of the polar front, Subantarctic front, and subtropical front, respectively, whereas PF, SAF, and STF report the position of the isotherms of the present-day polar front, Subantarctic front and subtropical front, respectively.

the source area of the icebergs, the iceberg frequency, and by calving processes [*Ehrmann*, 1991]. For these reasons there is no correlation between the magnitude of the IRD signal and the SSST values. We found increased IRD values at the transitions from interglacials to glacials cooccurring with benthic oxygen isotope values that translate to a sea level of ca. 50–70 m below present. This suggests that a drop in sea level that is dated to Northern Hemisphere ice sheet development, controls the production of Antarctic icebergs that carry terrigenous debris. Moreover, the IRD record is more or less in phase with the benthic $\delta^{18}O$ in the eccentricity cycle (Table 4). This relationship might indicate a close relationship between the Northern Hemisphere ice volume fluctuations and the production of Antarctic icebergs, recorded through the IRD occurrence. The role of the sea level in the occurrence of IRD has already been proposed [*Watkins et al.*, 1982; *Ehrmann*, 1991; *Ehrmann et al.*, 1991; *Warnke and Allen*, 1991; *Kanfoush et al.*, 2000].

[25] A different pattern is observed in the late glacial periods where high IRD values decrease to near-zero values during terminations. This can be explained by rapidly increasing SSST that exclude the invasion of icebergs into the modern Subantarctic realm already before or at the very onset of sea-level rise (Figure 8d). This offset is linked to the 3.3–6.5 kyr lead of Southern Ocean SSST versus the Northern Hemisphere ice volume change and sea level. In more southerly locations with lower SSST the maximum IRD input occurs at the terminations in relation with increasing sea level and massive discharge of Antarctic ice into the Southern Ocean (e.g., cores PS2319-1, PS2515-3: *Diekmann et al.* [2000]; Ocean Drilling program (ODP) Sites 745, 746: *Ehrmann and Grobe* [1991]). This results in a diachronous termination of IRD deposition in the Southern Ocean, depending on the latitude and surface water temperature regime, a model that was already proposed by *Keany et al.* [1976].

[26] The comparison of foraminiferal SSST records obtained from the Atlantic (this paper) and Indian sector of the Southern Ocean [*Howard and Prell*, 1992] permits the reconstruction of latitudinal variations of isotherms and related oceanographic fronts over a broader geographical area (Figure 9). The amplitude of SSST variations between glacial and interglacial periods is not always of the same order between our results and the records presented by *Howard and Prell* [1992], a pattern that might be related to lower time resolution obtained from the Indian cores or to the used reference data set. However, the general covariation of the SSST fluctuations in the Southern Atlantic and the Indian cores during the past ca. 450 kyr indicates that the isotherms in both sectors of the Southern Ocean have been displaced rather uniformly. A steepening of the temperature gradients most likely occurred near the present position of the STF where low temperature variations between glacial and interglacial periods were observed [*Prell et al.*, 1979]. Apparently, also in the Indian sector a dissolution-related increase of *G. inflata* results in rather high and overestimated SSST values in MIS 11, as documented in E49-17 [*Howard and Prell*, 1992]. Considering that the foraminiferal SSST estimations obtained

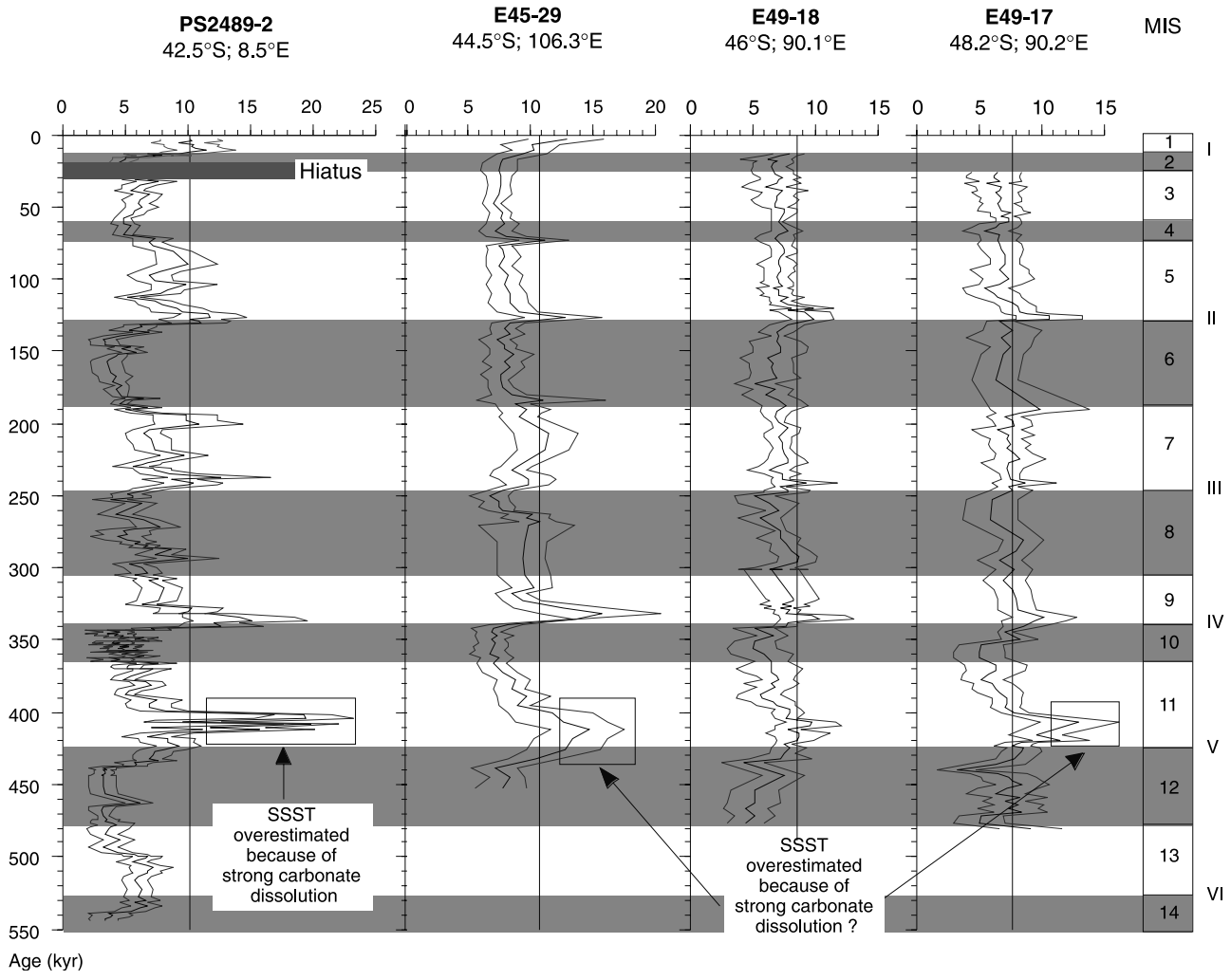

Figure 9. Comparison of the SSST estimated with the MAT in the South Atlantic (PS2489-2) and Indian Ocean records (E45-29, E49-18, E49-17) [*Howard and Prell*, 1992]. Vertical lines represent the present-day SSST for each core location. Shaded areas mark glacial periods. Terminations I–VI are labeled.

for MIS 11 result in overestimated values, MIS 9.3 most likely represents the warmest interglacial during the past 550 kyr.

4.2. Comparison with the Vostok Ice Core Record

[27] The 420 kyr record of atmospheric composition and temperature obtained from the Vostok ice core [*Petit et al.*, 1999] permits a comparison between oceanographic and atmospheric variability during the last four climate cycles. To facilitate the comparison between both records and assuming that the Southern Ocean SSST and the air temperature over Antarctica covary [*Pichon et al.*, 1992; *Waelbroeck et al.*, 1995], we developed an age model for Vostok by correlating the δD with the PS2489-2 SSSTs. The obtained correlation coefficient is 0.84. For comparison of absolute temperature changes we used the ΔT_I record from Vostok, which represents the atmospheric temperature at the inversion level where precipitation forms. These values should be of larger geographical significance than ΔT_s, the temperature at the surface. To transform ΔT_s into ΔT_I, we used the relationship $\Delta T_I = 0.67\Delta T_S$ according to *Jouzel et al.* [1987] and *Petit et al.* [1999]. We compared ΔT_I with ΔSSST, the deviation of the estimated SSST from the modern SSST at the core location.

[28] Although core PS2489-2 cannot resolve all rapid oscillations documented in the Vostok record, broad similarities are observed between the Vostok ΔT_I and the ΔSSST records (Figure 10). Most major temperature fluctuations are of similar amplitude in both the Vostok and the Subantarctic records. The drops in temperature during all glacial periods are more or less identical in both records as well as for cold interglacial periods such as around 228 kyr (MIS 7.4) and 107 kyr (MIS 5.4). During both periods, high deuterium excess rates have been reported from the Vostok ice core [*Jouzel et al.*, 1996; *Vimeux et al.*, 1999]. This was interpreted to signal significant differences in the hydrological cycle within a cold stage following an interglacial climatic optimum. *Vimeux et al.* [1999] suggested that during MIS 5.4 and MIS 7.4 the contribution of low-latitude

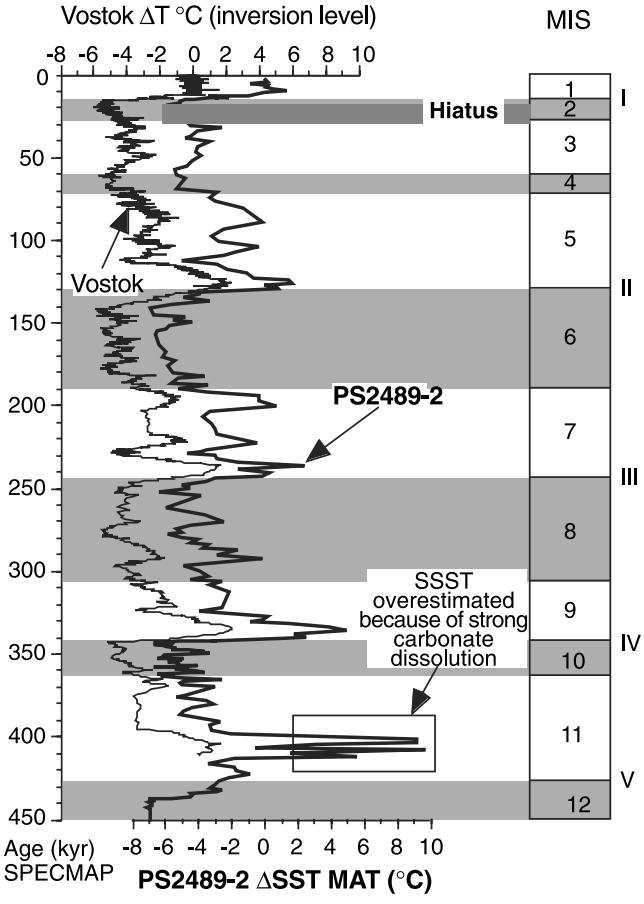

Figure 10. Comparison of the ΔT_I from the Vostok ice core (gray line) [*Petit et al.*, 1999] with the ΔSSST from the core PS2489-2 (dark line). Shaded areas mark glacial periods. Note that the temperature scales are similar but shifted to facilitate the comparison. Diagonal lines show the hiatus in the core PS2489-2. Terminations I–VI are labeled.

moisture to Antarctic precipitation was maintained at its interglacial level while the southern high-latitude oceans were a less-efficient source because they were cooled down. Such an interpretation is corroborated by our results that indicate a decrease in SSST to near-glacial values during MIS 5.4 and MIS 7.4 (Figure 10).

[29] During the interglacial climatic optima, both the ice and the sediment records show similar temperature increases. Temperatures of 1°–2°C higher than present, occur at around 238 kyr (MIS 7.5), 122 kyr (MIS 5.5), and 10 kyr (MIS 1 climatic optimum). During MIS 11.3 (around 405 kyr) and MIS 9.3 (around 331 kyr) the marine ΔSSST increase exceeds the ice core values. As discussed previously (section 3.1), the marine SSST estimates for MIS 11.3 are biased by selective dissolution of the foraminiferal assemblages and thus result in unrealistic values. However, the marine SSST values obtained for MIS 9.3 are rather realistic and show temperatures comparable to the atmospheric. MIS 9.3 was the warmest during the past 420 kyr, a pattern that is consistent with the occurrence of maximum atmospheric greenhouse gas concentrations (CH_4, CO_2) during this period [*Petit et al.*, 1999].

5. Conclusions

[30] The study of Subantarctic core PS2489-2 and its comparison with cores from the Indian Ocean and with the Vostok ice core allowed us to reconstruct the environment of the Southern Ocean during the last 550 kyr. Our findings can be summarized as follows:

1. During most past of the 550 kyr, the Southern Ocean SSSTs were lower than at present. Only during climatic optima (early Holocene, MIS 5.5, 7.1, 7.5, 9.3, and presumably also during MIS 11.3) are the SSSTs above modern SSST (by 1°–5°C). This suggests that the ACC zones and related oceanic frontal systems were shifted to a more northward position by up to 7° latitude rather uniformly in both the Atlantic and Indian sectors of the Southern Ocean.

2. Carbonate dissolution may have biased the SSST estimates by increasing the relative abundance of cold-water dwellers (*N. pachyderma*) or warm water dissolution-resistant species (*G. inflata*). This occurs during late MIS 13 and MIS 11 leading to underestimated SSST and during MIS 11.3, leading to overestimated SSST. Comparison of the glacial SSST with the IRD record indicates that despite increased fragmentation the preserved foraminiferal assemblages reflect well the glacial SSST values.

3. The relationship between IRD and benthic $\delta^{18}O$ at the transitions from interglacials to glacials suggests that a drop in sea level, due to Northern Hemisphere ice sheet development controls the production of Antarctic icebergs that carry terrigenous debris. However, the northern limit of IRD occurrence is confined to SSST around 4°C, as it has been shown from the modern iceberg distribution in the Atlantic sector of the Southern Ocean.

4. The 3.3–6.5 kyr lead of SSST versus the benthic $\delta^{18}O$ indicates that the initiation of warming in southern high latitudes heralds the start of deglaciation in the Northern Hemisphere. The planktic $\delta^{18}O$ and IRD records are strongly influenced by ice volume changes.

5. Broad similarities are observed between the core PS2489-2 and Vostok temperature records. Both records show that MIS 9.3 was the warmest period during the past 420 kyr, a pattern that is consistent with the occurrence of maximum atmospheric greenhouse gas concentrations during this period [*Petit et al.*, 1999]. The drops in SSST during the cold interglacial periods MIS 7.4 (228 kyr) and MIS 5.4 (107 kyr) are possibly related to low atmospheric temperatures associated with high deuterium excess at the same periods [*Vimeux et al.*, 1999].

[31] **Acknowledgments.** We thank S. Niebler, M.E. Salvignac, M. Labracherie, and J. Duprat for sharing the reference database, and A. Mackensen and M. Rutgers v.d. Loeff for fruitful discussions. We are grateful to R. Schneider for constructive comments on the first draft and J.A. Flores for the review of the last draft. Critical reviews of J. Cullen, D.A. Hodell, and an anonymous reviewer are acknowledged. Isotope measurements have been accomplished in the AWI isotope laboratory under the helpful guidance of A. Mackensen. This research was supported by the European grant CHRX-CT94-0424, the Sonderforschungsbereich 261, and by the Spanish government grant SB2000-0093.

References

Abelmann, A., and R. Gersonde, Biosiliceous particle flux in the Southern Ocean, *Mar. Chem.*, *35*, 503–536, 1991.

Abelmann, A., U. Brathauer, R. Gersonde, R. Sieger, and U. Zielinski, Radiolarian-based transfer function for the estimation of sea surface temperatures in the Southern Ocean (Atlantic sector), *Paleoceanography*, *14*, 410–420, 1999.

Bard, E., Correction of accelerator mass spectrometry ^{14}C ages measured in planktonic foraminifera: Paleoceanographic implications, *Paleoceanography*, *3*(6), 635–645, 1988.

Bauch, H. A., H. Erlenkeuser, J. P. Helmke, and U. Struck, A paleoclimatic evaluation of marine oxygen isotope stage 11 in the high-northern Atlantic (Nordic seas), *Global Planet. Change*, *24*, 27–39, 2000.

Becquey, S., and R. Gersonde, Past hydrographic and climatic changes in the Subantarctic zone of the South Atlantic-The Pleistocene record from ODP Site 1090, *Palaeogeogr. Palaeoclimatol. Palaeoecol.*, *182*, 221–239, 2002.

Berger, W. H., Planktonic foraminifera: Selective solution and paleoclimatic interpretation, *Deep Sea Res.*, *15*, 31–43, 1968.

Berger, W. H., Planktonic foraminifera: Selective solution and the lysocline, *Mar. Geol.*, *8*, 111–138, 1970.

Boyle, E. A., and L. Keigwin, North Atlantic thermohaline circulation during the past 20,000 years linked to high-latitude surface temperature, *Nature*, *330*, 35–40, 1987.

Brathauer, U., and A. Abelmann, Late Quaternary variations in sea surface temperatures and their relationship to orbital forcing recorded in the Southern Ocean (Atlantic sector), *Paleoceanography*, *14*, 135–148, 1999.

Broecker, W. S., Glacial to interglacial changes in ocean history, *Prog. Oceanogr.*, *11*, 151–197, 1982a.

Broecker, W. S., Ocean chemistry during glacial time, *Geochim. Cosmochim. Acta*, *46*, 1689–1705, 1982b.

Curry, W. B., J. C. Duplessy, L. D. Labeyrie, and N. J. Shackleton, Changes in the distribution of $\delta^{13}C$ of deep water $\sum CO_2$ between the last glaciation and the holocene, *Paleoceanography*, *3*(3), 317–341, 1988.

Diekmann, B., G. Kuhn, V. Rachold, A. Abelmann, U. Brathauer, D. K. Fütterer, G. Gersonde, and H. Grobe, Terrigenous sediment supply in the Scotia Sea (Southern Ocean): Response to late Quaternary ice dynamics in Patagonia and on the Antarctic peninsula, *Palaeogeogr. Palaeoclimatol. Palaeoecol.*, *162*, 357–387, 2000.

Donner, B., and G. Wefer, Flux and stable isotope composition of *Neogloboquadrina pachyderma* and other planktonic foraminifers in the Southern Ocean (Atlantic sector), *Deep Sea Res.*, *41*, 1733–1743, 1994.

Duplessy, J. C., and N. J. Shackleton, Response of global deep-water circulation to Earth's climatic change 135,000–107,000 years ago, *Nature*, *316*, 500–507, 1985.

Duplessy, J. C., N. J. Shackleton, R. G. Fairbanks, L. D. Labeyrie, D. Oppo, and N. Kallel, Deepwater source variations during the last climatic cycle and their impact on the global deepwater circulation, *Paleoceanography*, *3*(3), 343–360, 1988.

Ehrmann, W. U., Implications of sediment composition on the southern Kerguelen plateau for paleoclimate and depositional environment, *Proc. Ocean Drill. Program Sci. Results*, *119*, 185–203, 1991.

Ehrmann, W. U., and H. Grobe, Cyclic sedimentation at Sites 745 and 746, *Proc. Ocean Drill. Program Sci. Results*, *119*, 225–237, 1991.

Ehrmann, W. U., H. Grobe, and D. K. Fütterer, Late Miocene to Holocene glacial history of East Antarctica revealed by sediments from Sites 745 and 746, *Proc. Ocean Drill. Program Sci. Results*, *119*, 239–251, 1991.

Fischer, G., R. Gersonde, and G. Wefer, Organic carbon, biogenic silica and diatom fluxes in the marginal winter sea-ice zone and in the Polar Front Region: Interannual variations and differences in composition, *Deep Sea Res., Part II*, *49*(9–10), 1721–1745, 2002.

Gersonde, R., Die Expedition ANTARKTIS-XI/2 mit FS "*Polarstern*" 1993/94, *Rep. Polar Res.*, 163, 133 pp., 1995.

Gersonde, R., A. Abelmann, U. Brathauer, R. Sieger, and U. Zielinski, Das Südpolarmeer-ein Schlüsselgebiet für Klimaänderungen in vergangener Zeit, *Geowissenschaften*, *14*, 365–369, 1996.

Hodell, D. A., C. D. Charles, and U. S. Ninnemann, Comparison of interglacial stages in the South Atlantic sector of the Southern Ocean for the past 450 kyrs: Implications for marine isotope stage (MIS) 11, *Global Planet. Change*, *24*, 7–26, 2000.

Hodell, D. A., C. D. Charles, and F. J. Sierro, Late Pleistocene evolution of the ocean's carbonate system, *Earth Planet. Sci. Lett.*, *192*, 10–124, 2001.

Howard, W. R., and W. L. Prell, A comparison of radiolarian and foraminiferal paleoecology in the southern Indian Ocean: New evidence for the interhemispheric timing of climatic change, *Quat. Res.*, *21*, 244–263, 1984.

Howard, W. R., and W. L. Prell, Late Quaternary surface circulation of the southern Indian Ocean and its relationship to orbital variations, *Paleoceanography*, *7*(1), 79–117, 1992.

Hut, G., Consultants group meeting on stable isotope reference samples for geochemical and hydrological investigations, in *Rep. to Directory of Geneva International Atomic Energy Agency*, *42*, Vienna, 1987.

Hutson, W. H., Variations in planktonic foraminiferal assemblages along North–South transects in the Indian Ocean, *Mar. Micropaleontol.*, *2*, 47–66, 1977.

Hutson, W. H., Agulhas current during the late Pleistocene: Analysis of modern faunal analogs, *Science*, *207*, 64–66, 1980.

Imbrie, J., J. D. Hays, D. G. Martinson, A. McIntyre, A. C. Mix, J. J. Morley, N. G. Pisias, W. L. Prell, and N. J. Shackleton, The orbital theory of Pleistocene climate: Support from a revised chronology of the marine $\delta^{18}O$ record, in *Milankovitch and Climate*, part I, edited by A. Berger et al., pp. 269–305, D. Reidel, Norwell, Mass., 1984.

Jenkins, G. M., and D. G. Watts, *Spectral Analysis and its Applications*, Holden-Day, Boca Raton, Fla., 523 pp., 1968.

Jouzel, J., C. Lorius, J. R. Petit, J. C. Genthon, N. I. Barkov, V. M. Kotlyakov, and V. M. Petrov, Vostok ice core: A continuous isotope temperature record over the last climatic cycle (160,000 years), *Nature*, *329*, 403–408, 1987.

Jouzel, J., et al., Climatic interpretation of the recently extended Vostok ice records, *Clim. Dyn.*, *12*, 513–521, 1996.

Kanfoush, S. L., D. A. Hodell, C. D. Charles, T. P. Guilderson, P. G. Mortyn, and U. S. Ninnemann, Millennial-scale instability of the Antarctic Ice Sheet during the last glaciation, *Science*, *288*, 1815–1818, 2000.

Keany, J., M. Ledbetter, N. Watkins, and T. C. Huang, Diachronous deposition of ice-rafted debris in Subantarctic deep-sea sediments, *Geol. Soc. Am. Bull.*, *87*, 873–882, 1976.

Keir, R. S., On the last Pleistocene ocean chemistry and circulation, *Paleoceanography*, *3*(4), 413–445, 1988.

Kunz-Pirrung, M., R. Gersonde, and D. A. Hodell, Mid-Brunhes century-scale diatom sea surface temperature and sea ice records from the Atlantic sector of the Southern Ocean (ODP Leg 177, Sites 1093, 1094 and core PS2089-2), *Palaeogeogr. Palaeoclimatol. Palaeoecol.*, *182*, 305–328, 2002.

Labeyrie, L., J. C. Duplessy, and P. L. Blanc, Variations in mode of formation and temperature of oceanic deep waters over the past 125,000 years, *Nature*, *327*, 477–482, 1987.

Labeyrie, L., et al., Hydrographic changes of the Southern Ocean (southeast Indian sector) over the last 230 kyr, *Paleoceanography*, *11*, 57–76, 1996.

Labracherie, M., L. Labeyrie, J. Duprat, E. Bard, M. Arnold, J. J. Pichon, and J. C. Duplessy, The last deglaciation in the Southern Ocean, *Paleoceanography*, *4*(6), 629–638, 1989.

Le, J., and N. J. Shackleton, Carbonate dissolution fluctuations in the western equatorial Pacific during the late Quaternary, *Paleoceanography*, *7*(1), 21–42, 1992.

Levitus, S., and T. Boyer, *World Ocean Atlas,* vol. 4, *Temperature*, *NOAA Atlas NESDIS 4*, U.S. Dept. of Commerce, Washington, D. C., 1994.

Lutjeharms, J. R. E., Location of frontal systems between Africa and Antarctica: Some preliminary results, *Deep Sea Res.*, *32*, 1499–1509, 1985.

Lutjeharms, J. R. E., and H. R. Valentine, Southern Ocean thermal fronts south of Africa, *Deep Sea Res.*, *31*, 1461–1475, 1984.

McManus, J. F., D. W. Oppo, and J. L. Cullen, A 0.5-million-year record of millennial-scale climate variability in the North Atlantic, *Science*, *283*, 971–975, 1999.

Morley, J. J., Variations in high-latitude oceanographic fronts in the southern Indian Ocean: An estimation based on faunal changes, *Paleoceanography*, *4*(5), 547–554, 1989.

Nadeau, M. J., M. Schleicher, P. M. Grootes, H. Erlenkeuser, A. Gottdang, D. J. W. Mous, M. Sarnthein, and H. Willkomm, The Leibniz-Labor AMS facility at the Christian-Albrechts University, Kiel, Germany, *Nucl. Instrum. Methods Phys. Res., Sect. B*, *123*, 22–30, 1997.

Niebler, H. S., and R. Gersonde, A planktic foraminiferal transfer function for the southern South Atlantic Ocean, *Mar. Micropaleontol.*, *34*, 213–234, 1998.

Niebler, H. S., H. W. Hubberten, and R. Gersonde, Oxygen isotope values of planktic foraminifera: A tool for the reconstruction of surface water stratification, in *Use of Proxies in Paleoceanography: Examples from the South Atlantic*, edited by G. Fisher and G. Wefer, pp. 165–189, Springer-Verlag, New York, 1999.

Olbers, D., V. Gouretski, G. Seib, and J. Schröter, *Hydrographic Atlas of the Southern Ocean 82S*, Alfred Wegener Inst., Bremerhaven, 1992.

Oppo, D. W., and R. G. Fairbanks, Variability in the deep and intermediate water circulation of the Atlantic Ocean during the past 25,000 years: Northern Hemisphere modulation of the Southern Ocean, *Earth Planet. Sci. Lett.*, *86*, 1–15, 1987.

Oppo, D. W., J. F. McManus, and J. L. Cullen, Abrupt climate events 500,000 to 340,000 years ago: Evidence from subpolar North Atlantic sediments, *Science*, *279*, 1335–1338, 1998.

Overpeck, J. T., T. Webb III, and I. C. Prentice, Quantitative interpretation of fossil pollen spectra: Dissimilarity coefficients and the method of modern analogs, *Quat. Res.*, *23*, 87–108, 1985.

Paillard, D. L., L. Labeyrie, and P. Yiou, Macintosh program performs time-series analysis, *Eos Trans. AGU*, *77*, 379, 1996.

Peterson, R. G., and L. Stramma, Upper-level circulation in the South Atlantic Ocean, *Prog. Oceanogr.*, *26*, 1–73, 1991.

Petit, J. R., et al., Climate and atmospheric history of the past 420,000 years from the Vostok ice core, Antarctica, *Nature*, *399*, 429–436, 1999.

Pflaumann, U., J. Duprat, C. Pujol, and L. Labeyrie, SIMMAX: A modern analog technique to deduce Atlantic sea surface temperatures from planktonic foraminifera in deep-sea sediments, *Paleoceanography*, *11*, 15–35, 1996.

Pichon, J. J., L. D. Labeyrie, G. Bareille, M. Labracherie, J. Duprat, and J. Jouzel, Surface water temperature changes in the high latitudes of the Southern Hemisphere over the last glacial-interglacial cycle, *Paleoceanography*, *7*(3), 289–318, 1992.

Prell, W. L., W. H. Hutson, and D. F. Williams, The subtropical convergence and late Quaternary circulation in the southern Indian Ocean, *Mar. Micropaleontol.*, *4*, 225–234, 1979.

Prentice, I. C., Multidimensional scaling as a research tool in Quaternary palynology: A review of theory and methods, *Rev. Palaeobot. Palynol.*, *31*, 71–104, 1980.

Raymo, M. E., W. F. Ruddiman, N. J. Shackleton, and D. W. Oppo, Evolution of Atlantic-Pacific $\delta^{13}C$ gradients over the last 2.5 m.y., *Earth Planet. Sci. Lett.*, *97*, 353–368, 1990.

Sarnthein, M., K. Winn, S. J. A. Jung, J. C. Duplessy, L. Labeyrie, H. Erlenkeuser, and G. Ganssen, Changes in East Atlantic deepwater circulation over the last 30,000 years: Eight time slice reconstructions, *Paleoceanography*, *9*, 209–268, 1994.

Sea Ice Climatic Atlas, vol. 1, *Antarctic*, Naval Oceanogr. Command Detachment, Asheville, NSTL, p. 131, 1985.

Shackleton, N. J., Attainment of isotopic equilibrium between ocean water and the benthonic foraminifera genus *Uvigerina*: Isotopic changes in the ocean during the last glacial, *Cent. Natl. Rech., Sci. Coloq. Int.*, *219*, 183–190, 1974.

Sieger, R., Dokumentation MacMAT-Modern Analog Technique, available at www.pangaea.de, 1995.

Sieger, R., R. Gersonde, and U. Zielinski, A new extended software package for quantitative paleoenvironmental reconstructions, *Eos Trans. AGU*, *80*, 223, 1999.

Thiede, J., S. Nees, H. Schulz, and P. De Deckker, Oceanic surface conditions recorded on the sea floor of the southwest Pacific Ocean through the distribution of foraminifers and biogenic silica, *Palaeogeogr. Palaeoclimatol. Palaeoecol.*, *131*, 207–239, 1997.

Thunell, R. C., and S. Honjo, Calcite dissolution and the modification of planktonic foraminiferal assemblages, *Mar. Micropaleontol.*, *6*, 169–182, 1981.

Vimeux, F., V. Masson, J. Jouzel, M. Stievenard, and J. R. Petit, Glacial-interglacial changes in ocean surface conditions in the Southern Hemisphere, *Nature*, *398*, 410–413, 1999.

Waelbroeck, C., J. Jouzel, L. Labeyrie, C. Lorius, M. Labracherie, M. Stiévenard, and N. I. Barkov, A comparison of the Vostok ice deuterium record and series from Southern Ocean core MD 88-770 over the last two glacial-interglacial cycles, *Clim. Dyn.*, *12*, 113–123, 1995.

Waelbroeck, C., M. Labracherie, J. L. Turon, and L. Labeyrie, Southern Ocean core MD94-101, *PAGES Newsl.*, *7*, 9, 1999.

Warnke, D. A., and C. P. Allen, Ice rafting, glacial-marine sediments, and siliceous oozes: South Atlantic/Subantarctic Ocean, *Proc. Ocean Drill. Program Sci. Results*, *114*, 589–598, 1991.

Watkins, N. D., M. T. Ledbetter, and T. C. Huang, Antarctic glacial history using spatial and temporal variations of ice-rafted debris in abyssal sediments of the Southern Ocean, in *Antarctic Geoscience*, edited by C. Craddock, pp. 1013–1016, Univ. of Wis. Press, Madison, 1982.

Weaver, P. P. E., H. Neil, and L. Carter, Sea surface temperature estimates from the Southwest Pacific based on planktonic foraminifera and oxygen isotopes, *Palaeogeogr. Palaeoclimatol. Palaeoecol.*, *131*, 241–256, 1997.

Weaver, P. P. E., L. Carter, and H. L. Neil, Response of surface water masses and circulation to late Quaternary climate change east of New Zealand, *Paleoceanography*, *13*(1), 70–83, 1998.

Wefer, G., and G. Fischer, Annual primary production and export flux in the Southern Ocean from sediment trap data, *Mar. Chem.*, *35*, 597–614, 1991.

Wefer, G., G. Fischer, D. Fütterer, and R. Gersonde, Seasonal particle flux in the Bransfield Strait, *Antarctica, Deep Sea Res.*, *35*, 891–898, 1988.

Zielinski, U., and R. Gersonde, Diatom distribution in Southern Ocean surface sediments: Implications for paleoenvironmental reconstructions, *Palaeogeogr. Palaeoclimatol. Palaeoecol.*, *129*, 213–250, 1997.

S. Becquey, Department of Geology, Faculty of Sciences, University of Salamanca, 37008, Salamanca, Spain. (becquey@usal.es)

R. Gersonde, Alfred-Wegener Institute for Polar and Marine Research, Columbusstrasse, 27515, Bremerhaven, Germany.